Journal of Materials Chemistry A

Accepted Manuscript

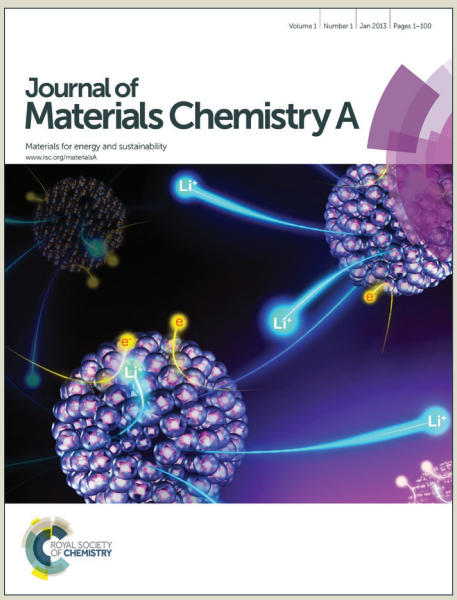

ROYAL SOCIETY OF CHEMISTRY

www.rsc.org/materialsA

Green energy storage chemistries based on neutral aqueous electrolytes

Zheng Chang, Yaqiong Yang, Minxia Li, Xiaowei Wang and Yuping Wu*

DOI: 10.1039/b000000x [DO NOT ALTER/DELETE THIS TEXT]

Widespread use of the fossil fuels has resulted in many environmental problems. It is urgent to search for reliable green energy storage technologies. The electrical energy storage systems based on neutral aqueous solutions are attractive candidates compared to the present energy storage systems utilizing flammable and expensive organic electrolytes because of their instinct improved safety, low cost and environmental friendliness. What's more, the high-rate performance can be achieved due to the high ionic conductivity of the aqueous electrolytes. However, the lower electrochemical window of water limits the possible high output voltage and high energy density. Recently, many new concepts based on neutral aqueous energy storage chemistries including aqueous rechargeable batteries and supercapacitors have exhibited high power and energy densities, excellent cycling life and high Coulomb efficiency. The present work reviews the latest advances on these new chemistries based on the neutral aqueous electrolytes, and the challenges and outlooks in this field are briefly commented on and discussed.

* New Energy and Materials Laboratory (NEML), Department of Chemistry and Shanghai Key Laboratory of Molecular Catalysis and Innovative Materials, Fudan University, No. 220, Handan Road, Shanghai 200433, China. E-mail: wuyp@fudan.edu.cn; Tel: +86-21-55664223; Fax: +86-21-55664223

1 Introduction

Recently, the rapid depletion of the fossil fuels and the increasing emission of greenhouse gases causing air pollution have become a serious issue. There is a clear urgent need for the development of reliable green energy storage technologies to achieve a secured and reliable energy supply. Electrical energy storage (EES) system including batteries and supercapacitors, an intermediate platform to the versatile and efficient deployment of renewable energy such as solar, wind and tide, has received worldwide concern. What's more, they play a prominent role in our future modern lives. Since the emergence and extensive use of such many new types of portable electronic devices and electric vehicles (EVs) which are promisingly expected to significantly contribute to solving the problems of global warming and environmental pollution, the demand for good EES systems is becoming more and more urgent [1-5].

Lithium ion batteries (LIB) have been well acknowledged as an EES system with high energy density and long cycling life, which are superior to other conventional batteries [6-10]. However, their inherent safety issue related to the use of high cost, toxic and flammable organic electrolyte and superfast charging performance are still two challenges for their applications in large-scale EES systems such as electric vehicles and smart grids[11, 12]. Compared with the combustible organic electrolytes of LIBs, operating in environmentally friendly neutral aqueous electrolytes with high ionic conductivity, about 2 orders of magnitudes higher than those of the nonaqueous ones, is attractive for electrochemical energy storage in terms of safety and cost[13-16]. If both high specific power and energy densities are achieved, such EESs would be useful for power quality applications such as to assist propelling electric vehicles that require fast acceleration and intense braking [17]. Nevertheless, the previous energy storage devices using aqueous electrolytes based on different chemistries such as Ni-Cd, Ni-MH and lead acid batteries are limited in applications due to their serious ecological threat, poor cycling life and low energy density [18-20]. There are a lot of endeavors to explore new EES systems [21-24].

Since 2007 aqueous rechargeable lithium batteries (ARLBs) using positive electrode materials from commercial LIBs have again attracted wide attentions as a promising system because of their low capital investment, environmental friendliness and good safety, which can be an alternative because their energy density can be above that of lithium ion batteries [14, 15, 25-30]. Different flexible EES systems based aqueous electrolytes sprang up in recent years: a variety of novel aqueous alkali-ion battery chemistries[31,33] and supercapacitors[32]. They are potentially advantageous owing to their good safety, high ionic conductivity and low cost of aqueous electrolytes.

In this review, we briefly discuss the recent progress and challenges associated with the EES systems based on neutral aqueous electrolytes including aqueous rechargeable batteries and supercapacitors with emphasis on the remarkable work.

1 Aqueous rechargeable batteries

Aqueous rechargeable batteries mainly include aqueous rechargeable lithium batteries (ARLBs) and aqueous rechargeable sodium and potassium batteries.

1.1 Aqueous rechargeable lithium batteries

As an ARLB, it should meet the following three conditions [14]:

(a) It uses lithium intercalation or lithium-containing compound(s) as one or two electrodes;

(b) Its charge and discharge processes are based on redox reactions accompanying the gain and loss of electrons instead of absorption and desorption;

(c) It uses lithium-containing aqueous solution as an electrolyte.

ARLBs can overcome some disadvantages of lithium ion batteries such as the high cost and safety problems, and environment pollution problems of lead acid or Ni–Cd batteries. It may be an ideal energy storage system to satisfy the demands of a grid-scale application due to its excellent safety and reliability [14, 34-36]. However, since the introduction of ARLBs in 1994, the progress on improving their performance was very limited. Recently, there are many breakthroughs which show clearly that they can present very high reversible capacity, good cycling performance, and rate capability especially super-fast charge performance which can be comparable with filling gasoline for engine cars [13-16, 28, 37-41]. Of course, they include positive and negative electrodes.

1.1.1 Positive electrode materials

There are various positive electrode materials for ARLBs, which are listed in Table 1, and their properties are also summarized in Table 1. To the best of our knowledge, spinel $LiMn_2O_4$ is considered to be an excellent candidate in ARLB due to its low cost, good stability and electrochemical performance in aqueous electrolytes. The cyclic voltammograms (CVs) of $LiMn_2O_4$ in 0.5 mol L^{-1} Li_2SO_4 aqueous solution and in an organic electrolyte are shown in Fig. 1 [38, 42]. There are two redox couples which are situated at 0.78/0.73 V and 0.92/0.83 V (vs. SCE), respectively, at the scan rate of 1 mV s^{-1}, attributed to lithium intercalation and deintercalation in the spinel host structure in the aqueous electrolyte. Additionally, the CVs in the aqueous electrolyte at the higher scan rates, even at 100 mV s^{-1}, present two couples of well defined and sharp redox peaks, which is much better than that in the organic electrolyte. In the case of the organic electrolyte, when the scan rate is increased to 2 mV s^{-1}, the two couples of redox peaks could not be differentiated. From the above comparison, it is clear that the current response and the reversibility of the redox behaviors in the aqueous electrolytes are better than those in the organic electrolytes due to the higher ionic conductivities of the aqueous electrolytes.

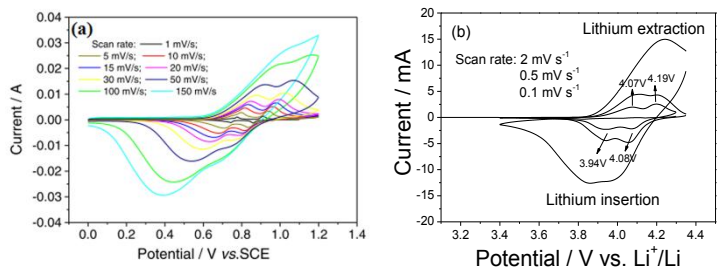

Fig.1 CV curves of $LiMn_2O_4$ in (a) 0.5 mol L^{-1} Li_2SO_4 aqueous electrolyte and (b) 1 mol L^{-1} $LiPF_6$ solution in a mixture of ethylene carbonate, diethyl carbonate and dimethyl carbonate (volume ratio: 1/1/1) (Modified from refs. 38 and 42.

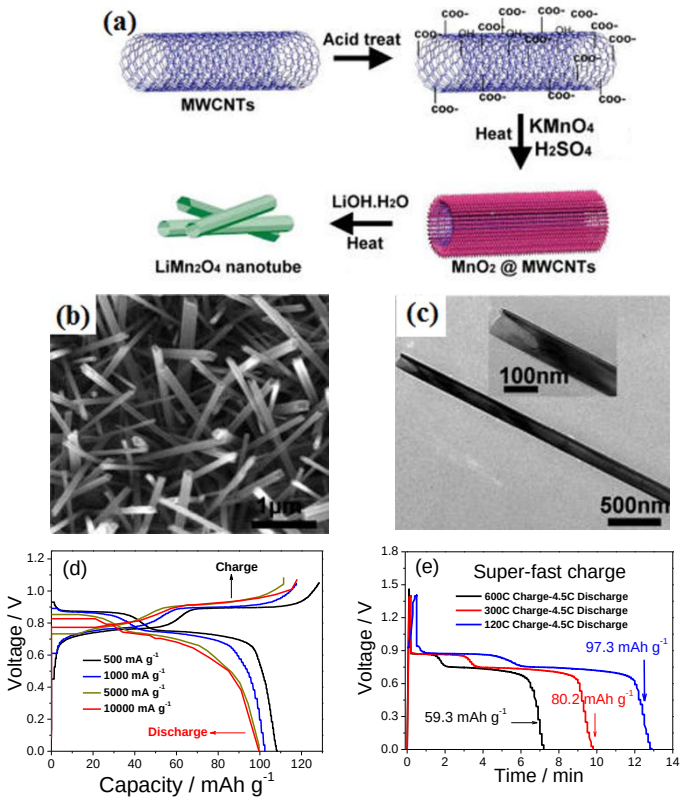

Fig.2 (a) Schematic process of the synthesis, (b) scanning electron micrograph, (c) transmission electron micrograph, (d) charging and discharging curves at different current densities, and (e) super-fast charge performance of the $LiMn_2O_4$ nanotube. Its electrochemical performance is measured using Ni as the counter electrode and SCE as the reference electrode (Modified from ref. 43).

The excellent cyclic voltammetric behavior in the aqueous electrolyte shows great promise for super-fast charge and discharge capabilities [13, 38, 43, 44]. In the case of a $LiMn_2O_4$ nanotube prepared by using multiwall carbon nanotubes as a sacrificial template, its schematic synthesis route, morphologies and electrochemical properties are shown in Fig. 2 [43]. It exhibits excellent rate behavior and displays a reversible capacity of 110 and 99 mA h g^{-1} at the charge/discharge current densities of 500 and 10 000 mA g^{-1}, respectively. The flat plateaus in the charge and discharge curves are well-defined at all current densities and the voltage decrease is very slight at very high current densities. The charge process of this positive electrode material can be finished within several seconds. Capacities of 97.3, 80.2 and 59.3 mAh g^{-1}, corresponding to 88.5% 72.9% and 53.9% of the capacity, respectively, could be obtained at the charging rates of 120C (30 s), 300C (12 s), and 600C (6 s). This superfast second-level charge capability can be ascribed to the following reasons: (1) The ionic conductivity of the aqueous electrolyte is much higher than that of the organic electrolytes; (2) The crystal orientation of the $LiMn_2O_4$ nanotube suggests that more Li sites are exposed to the aqueous electrolyte due to the preferred growth of (400) planes; and (3) the unique nanostructure leads to the low electronic

resistance and makes Li^+ ions deintercalate and intercalate very easily because of very short diffusion distance.

In the aqueous electrolytes, the Jahn-Teller effects still exist, which can be seen clearly from the charge and discharge curves as shown in Fig. 2d. However, porous structure can accommodate some strain/stress during the charge and discharge process. As shown in Fig.3, a porous $LiMn_2O_4$ prepared by using polystyrene particles as a template exhibits excellent cycling performance [13]. There is no more than 7% capacity loss after 10000 full cycles at 9C (1000 mA g^{-1}) in the neutral 0.5 mol L^{-1} Li_2SO_4 aqueous electrolyte. Such a result is markedly superior to those reported in the organic electrolytes. In contrast, the discharge capacity of the conventional solid $LiMn_2O_4$ electrode decreases rapidly at the first 2000 cycles. Only 19.8 mA h g^{-1} is retained after 10000 cycles. Moreover, other effective methods such as doping, surface coating can be utilized to improve the cycling behavior by buffering structural distortion during the charge/discharge process [41].

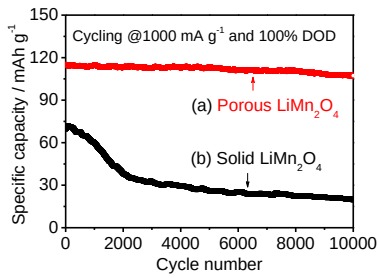

Fig.3 Cycling behavior of the (a) porous and (b) solid $LiMn_2O_4$ in 0.5 mol L^{-1} Li_2SO_4 aqueous electrolyte (Modified from ref. 13).

As mentioned above, nanostructure provides good performance for the positive electrode materials of ARLBs since the nanostructured materials could provide short diffusion pathways and more channels due to their high specific surface area for the intercalation/de-intercalation of Li^+ ions [13, 37, 45]. Recent studies on lithium intercalation materials have paid much attention to the nanostructured materials with various morphologies (Table 2) such as nanoporous [46-48], nanochains [44], nanotubes [43, 49, 50], nanowires [51], nanorods [52, 53], nanosheets [54] and so on. Further combination of nanostructures with traditional micrometer structures will push their further development.

1.1.2 Negative electrode materials

As to the negative electrode materials for ARLBs, vanadium oxides, molybdenum oxides and some lithium intercalation compounds have been reported, and some performances are also summarized in Table 1. Research about their negative electrode materials is quite limited owing to more challenges concerning dissolution of the active cations so that some conductive polymers or carbon are coated on the surface of negative electrode materials [45, 55-57] . It is well known that polypyrrole (PPy) is one of the most popular conducting polymers [58, 59], which has been used to modify electrode materials for lithium ion batteries. It not only serves as a conducting additive reducing the weight ratio of inert materials in the electrodes, but also acts as a coating prohibiting the dissolution of active material and associated release of metal ions during charge and discharge process.

For example, a hybrid of V_2O_5 nanowires and MWCNTs coated with PPy is

prepared as an anode material for ARLBs [56], and the preparation procedure is shown in Fig. 4a, which combines a hydrothermal method with chemical coating reaction. Its SEM and TEM micrographs (Figs. 4b and 4c) show that V_2O_5 nanowires are homogeneously entangled with MWCNTs to get a three-dimensional network structure, which is expected to provide a large interface with electrolytes for facile ion transportation and act as a conductive network with high electronic conductivity. The action mechanisms of the PPy coating and the MWCNTs are schematically shown in Fig. 4d. The PPy coating can prevent the dissolution of multivalent V^{n+} ions so that the electrochemical performance of the negative electrode material for the ARLB is markedly improved including the cycling life and rate capability.

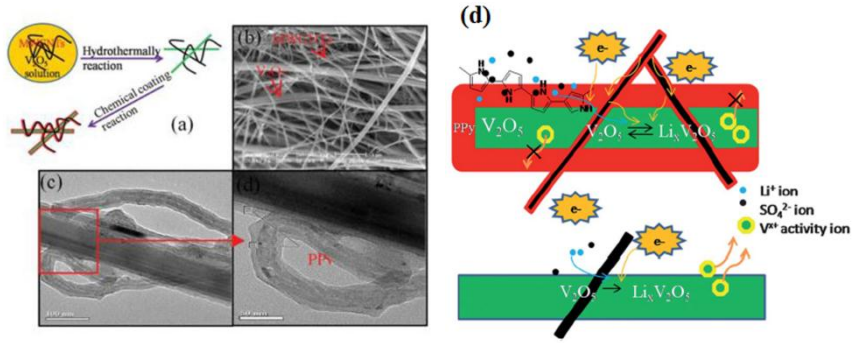

Fig.4 (a) Schematic preparation procedure of a hybrid of V_2O_5 nanowires and MWCNTs coated with PPy, (b) SEM micrograph of the virginal hybrid of V_2O_5 and MWCNTs, (c) TEM micrographs of the coated hybrid, and (d) the action of PPy to prevent the dissolution of V^{n+} cations during the charge and discharge process (Modified from ref. 56).

The lithium intercalation/de-intercalation processes and kinetic parameters of LiV_3O_8 as a negative electrode material for ARLBs are investigated by CV, chronoamperometry (CA), and electrochemical impedance spectroscopy (EIS) [60, 61]. There are also three steps of lithium ion intercalation reaction for LiV_3O_8 in the aqueous solution, agreeing well with those in the organic electrolyte. The rate capability of a nanorod LiV_3O_8 prepared by a sol–gel method, is very good. When it is further coated with a thin layer of PPy, its cycling behavior is also greatly ameliorated [55].

Metals such as Zn and Sn can also be used as negative electrode materials for the ARLBs since they can combine together with the positive electrode as mentioned above to achieve a higher discharge voltage and energy density [62-66].

1.1.3 Battery systems

Since Dahn's research group first reported an ARLB system with VO_2 and $LiMn_2O_4$ as negative and positive electrode materials, respectively, in 1994 [25], a lot of exploration on ARLB systems have been studied, which are listed in Table 3. Some properties are also summarized in Table 3. Here we take one example for illustration.

An ARLB consisting of a nanocomposite of PPy@MoO_3 and $LiMn_2O_4$ displays excellent rate capability and good cycling performance (Fig. 5) [45]. CV curves of the negative and positive electrodes in 0.5 mol L^{-1} Li_2SO_4 aqueous electrolyte at the

scan rate of 1 mV s^{-1} show that both of them are stable in aqueous electrolyte and can take place reversible redox reactions as shown in eq. (1):

$$LiMn_2O_4 + MoO_3 \underset{\text{Discharge}}{\overset{\text{Charge}}{\rightleftharpoons}} Li_{1-x}Mn_2O_4 + Li_xMoO_3 \qquad (1)$$

The electrochemical window of this ARLB can be up to 2.0 V. The charge cut-off voltage can be extended to 1.95 V without evident side reactions. In the charge and discharge curves, there are two evident plateaus, indicating clearly the redox reactions of $LiMn_2O_4$. The average charge and discharge voltages are 1.40 and 1.22 V, respectively. The cycling behavior of the ARLBs from the nanocomposite exhibits an improved cycling behavior compared with that from the virginal MoO_3 because that PPy coating can not only prevent or inhibit the dissolution of Mo ions but also buffer the possible volume changes during the cycling process. The energy density of this ARLB is 45 Wh kg^{-1} at 350 W kg^{-1} and even maintains at 38 Wh kg^{-1} at 6 kW kg^{-1}. This excellent rate capability can be compared with that of supercapacitors, which is ascribed to the nanochain structure of $LiMn_2O_4$ and the conductive PPy coating decreasing the charge transfer resistance.

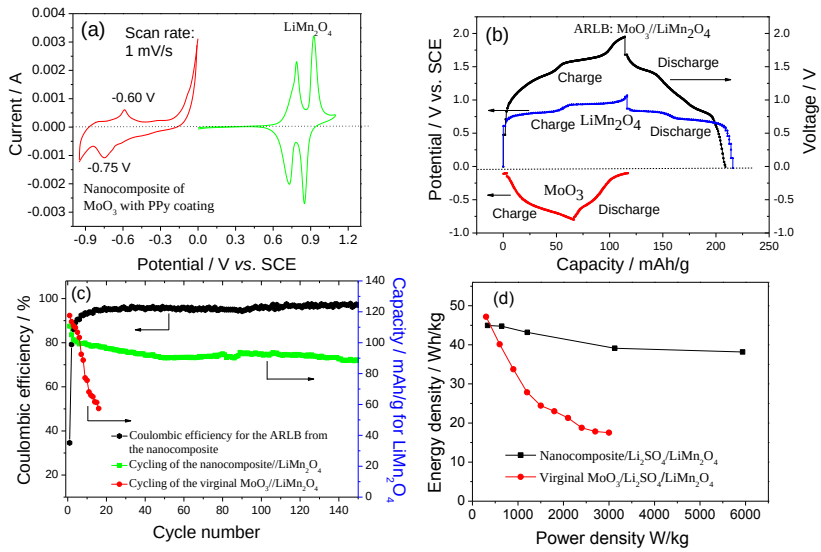

Fig.5 (a) CV curves of the nanocomposite of MoO_3 coated with PPy and the nanochain $LiMn_2O_4$ at the scan rate of 1 mV s^{-1}, (b) charge and discharge curves of the nanocomposite negative electrode, the nanochain $LiMn_2O_4$ positive electrode and the ARLB system consisting of the two electrodes, (c) the cycling behavior of the ARLBs at 1000 mA g^{-1} based on $LiMn_2O_4$, and (d) Ragone plots of the ARLBs system using 0.5 mol L^{-1} Li_2SO_4 aqueous solution (Modified from ref. 45).

When overpotentials are employed, the stable work voltage of ARLBs can be expanded leading to an increase in energy density. However, it is known that the electrochemical stable window is much narrow due to the decomposition of water, which is the main bottleneck for the further increase of the energy density of ARLBs. The output voltage could not be increased too high. Consequently, further direction is needed to break through this limit.

1.2 Aqueous rechargeable sodium and potassium batteries

The price of raw material in ARLBs could still be a bottleneck for large-scale EES systems, therefore aqueous rechargeable sodium batteries (ARSBs) appear to be an promising and attractive alternative to their lithium counterparts because of the wide availability and low cost of sodium resources [67]. However, ARSBs are rarely reported except a few of Na-intercalation materials. On the one hand, the radius of Na^+ (0.102 nm) especially hydrated sodium ion (0.358 nm) is much larger than those of H^+ and Li^+, making the intercalation reactions more difficult and leading to the low capacity of the active materials. On the other hand, bulky sodium ion during the intercalation leads to the deformation of lattice, resulting in the collapse of the crystal structure and poor cycling stability. In the case of aqueous rechargeable potassium batteries (ARPB), there are even less reports. Since they are batteries, they include positive and negative electrodes.

1.2.1 Positive electrode materials

Inspired by the positive electrode materials of ARLBs, some rich sodium (potassium) transition metal oxides such as birnessite type MnO_2, Na_xMnO_2, K_xMnO_2 can be used as the positive electrode materials. They present good reversible intercalation/deintercalation of sodium and potassium ions [68-71]. $Na_{0.44}MnO_2$[72,73,74] is used as a positive electrode with a high diffusion coefficient of about 10^{-13} – 10^{-12} cm^2 s^{-1}. It presents three pairs of redox peaks in the CV curves (Fig. 6), which are related to phase transitions. The optimized $Na_{0.44}MnO_2$ shows a specific capacity of 45 mAh g^{-1} with good cyclability for 1000 cycles. λ-MnO_2 is able to deliver a specific capacity up to 100 mA h g^{-1} [75].

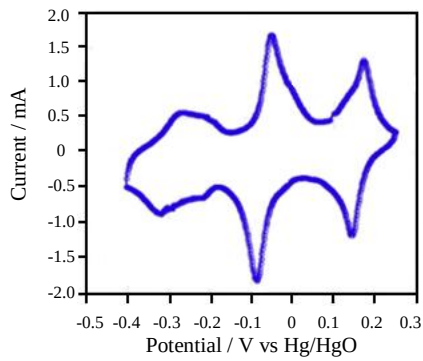

Fig.6 Cyclic voltammogram of the $Na_{0.44}MnO_2$ electrode material in 1 mol L^{-1} Na_2SO_4at the scan rate of 5 mV s^{-1}(Modified from ref. 73).

Prussian blue analogues with an open framework of general formula $A_xPR(CN)_6$ ($0 \leqslant x \leqslant 2$) in which P^{+m} and R^{+n} coordinate to the nitrogen and carbon ends of the CN-group, respectively, while A atoms can be intercalated in the interstitial sites that result from the large cages. Recently, proposed copper, nickel hexacyanoferrates ($KCuFe(CN)_6$ and $KNiFe(CN)_6$) and copper-nickel alloy hexacyanoferrate (CuNiHCF) materials offer ultra-long cycling life, high capacity, and very low hysteresis allowing the development of devices with very high energy efficiency for the positive electrodes of ARSBs and ARPBs and application for grid-scale energy storage [76-79]. Nanoparticles of sodium iron hexacyanoferrate are

employed as positive electrode materials for ARSBs [80]. These materials have a theoretical capacity up to 60 mAh g^{-1}. The discharge plateau of $KNiFe(CN)_6$ in the aqueous electrolyte is at 0.59 V (vs. SHE) for sodium ions, and 0.69 V for potassium ion, and that of $KCuFe(CN)_6$ is at 0.9 V and 0.95 V (vs. SHE) for sodium and potassium ions, respectively. What's more, the operating voltage of CuNiHCF is tunable based on its composition, which decreases dramatically with the increase of Ni content. The copper hexacyanoferrate has an ultra-low strain open framework structure, and presents excellent cycling behavior. After 40,000 deep discharge cycles at a 17 C rate, 83 % of the original capacity is retained [78]. Even at a very high cycling rate of 83 C, two thirds of its maximum discharge capacity is achieved. This good rate performance can be ascribed to the rapid kinetic behavior of Na^+ intercalation at modest current densities. The energy efficiencies can be up to 99%. In a word, it seems that the open framework structures of rigid MHCFs (M refers Cu, Ni, or their mixture) have greater durability compared to more extensively studied metal oxide electrode material [81].

1.2.2 Negative electrode materials

The sieving negative electrode materials with structural stability under low voltage for ARSBs and ARPBs is more difficult, and there are very limited reports. NASICON-type $NaTi_2(PO_4)_3$ can be seen a successful example [82,83]. CV and galvanostatic discharge/charge tests indicate that sodium can be reversibly intercalated into the host structure in the aqueous Na_2SO_4 solution, presenting stable charge and discharge platform at -0.82 V (vs. Ag/AgCl) with reversible capacity of 120 mAh g^{-1}, 70 % of the reversible capacity is retained even at 100C rate due to its fast ionic conductor structure of sodium. Some promising polymers such as polyimide and poly(2-vinylanthraquinone) can be used as the negative electrode for ARSBs [84, 85].

Zinc can be a good negative electrode since its redox potential is 0.13 V (vs. SHE) and its reversible redox reactions in the aqueous solution of $ZnAc_2$ and NaAc are very good [86], whose CV curves are shown in Fig.7. In the case of the positive electrode $Na_{0.95}MnO_2$, the de-intercalation and intercalation of Na^+ ions are not affected in the aqueous electrolyte.

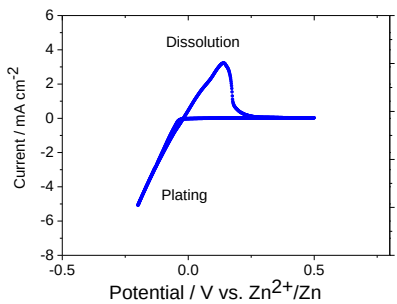

Fig.7 Cyclic voltamogramm of Zn in an aqueous solution of 0.5 mol L^{-1} $Zn(CH_3COO)_2$ and 0.5 mol L^{-1} CH_3COONa at the scan rate of 0.5 mV s^{-1}, which is tested by using platinum as the counter electrode (Modified from ref. 86).

1.2.3 Battery systems

From the above illustration, it is known that there are three types of negative electrode materials: oxides occurring redox reaction, transitional metal oxides based

on intercalation/deinercalation, and the metals Zn or Sn based on plating/dissolution during the charge and discharge processes. Some ARSBs are summarized in Table 4. Here we take the ARSB based on Zn and $Na_{0.95}MnO_2$ as one example [86]. Its charge and discharge process and some electrochemical performance is shown in Fig. 8. Its average discharge voltage is 1.4 V. It can be charged and discharged at high rate up to 15C at least, which can meet the rapid change of power supply and demand from the grids. Its energy density can be up to 78 Wh kg^{-1} based on the two electrode materials. Its cycling performance is very good with only 8% capacity loss after 1000 cycles at 4 C between 1 and 2 V.

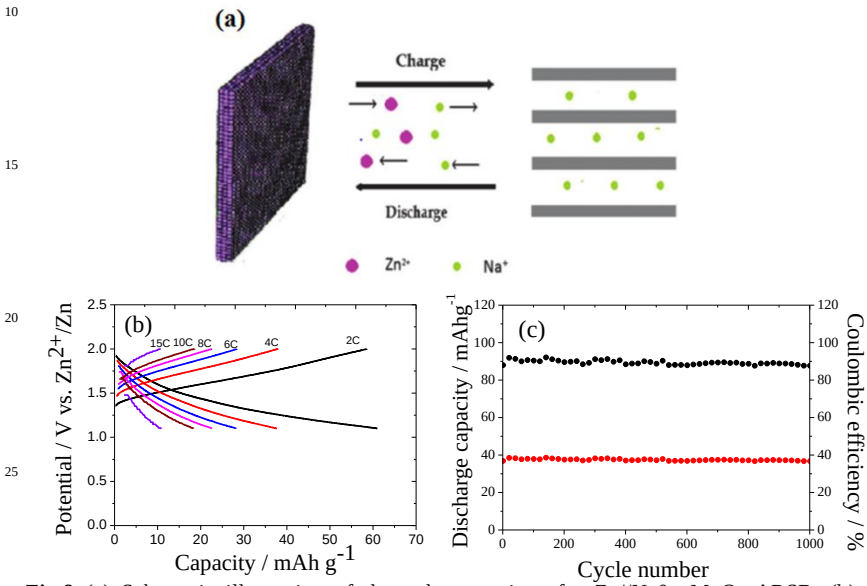

Fig.8 (a) Schematic illustration of the redox reactions for Zn//$Na_{0.95}MnO_2$ ARSB, (b) its charge and discharge curves at different rates, and (c) cycling performance 4 C rate with a fixed full charge capacity of 40 mA h g^{-1} based on $Na_{0.95}MnO_2$ (Modified from ref. 86).

1.3 High energy density ARLBs

The main disadvantage of the former mentioned ARLBs, which can be called as the first generation of ARLBs (1G ARLBs), is that their output voltage and energy density are still much lower than those of conventional lithium ion batteries due to the limit of the electrochemical stable window of water [14, 16, 28]. Since the output voltage of the new ARLBs is much higher above this window and can be above 4.0 V, these ARLBs are discussed in this separate section. Of course, it can also be called as second generation (2G) ARLBs. The main feature of these 2G ARLBs is that they use stable lithium metal as the negative electrode.

1.3.1 Stable lithium metal

If negative electrode materials of lower redox potentials can be stable in aqueous electrolytes, high energy density systems will be feasible. For the traditional ways, the removal of oxygen is very crucial [36]. Recently, our group invented a coated lithium metal that is stable in in neutral aqueous solution and the removal of oxygen is not needed [87-89]. It is well-known that alkali metals are very active, which belongs to "fire". Aqueous solutions surely belong to "water" in the traditional five elements

theory of China. It is known that fire and water are not compatible. To make them compatible, a "wood" is needed. Wood consists mostly of polymers. Then we put a layer of polymer (GPE) on the surface of lithium metal. The GPE consists of our home made sandwiched polymer membrane such as PVDF (poly(vinyl difluoride)) / PMMA (poly(methyl methacrylate)) / PVDF structuring with organic electrolyte. However, water molecules can slowly dissolve the lithium salt and organic solvents in the gel polymer electrolyte, and lithium ions cannot transport between the lithium metal and the aqueous solution. Another layer, glass-ceramic layer (LISICON from Ohara, Japan) which belongs to "earth", is used. LISICON film is a solid electrolyte ($\sigma_{Li+} > 10^{-4}$ S cm^{-1}) which can also act as a separator and allows only the pass-through of Li^+ ions between both sides of the film while the pass-through of protons, water, hydrated and solvated ions are forbidden. This composite layer makes lithium metal very stable, whose structure is schematically shown in Fig. 9a. In 0.5 mol L^{-1} Li_2SO_4 electrolyte, the coated lithium metal ensures the good electrochemical stability, only Li^+ ions can transfer between Li metal and the outside *via* the LISICON film and the GPE, and dissolution and plating of Li can reversibly happen at about -2.70 V (vs. SCE) (Fig. 9b). When Li metal is only coated by the membrane of the gel polymer electrolyte, the coated lithium metal is still stable in the aqueous solution even the temperature is up to 60°C.

The recent introduction of the solid electrolytes (LISICON) based on selective conduction of Li^+ ion paves a new way for constructing lithium batteries of high energy density by using Li-metal as the negative electrode [87-90]. Therefore, a new strategy for aqueous rechargeable batteries using water-soluble redox couples as the positive electrode or other positive electrodes is also possible.

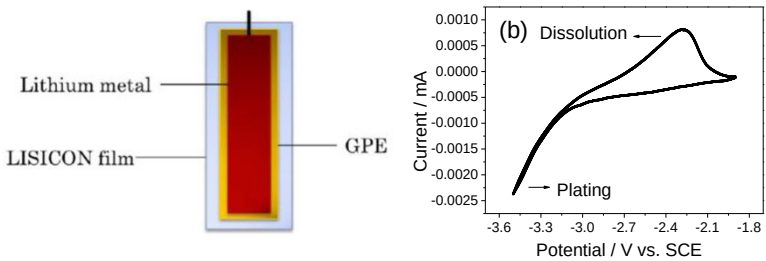

Fig.9 (a) Schematic illustration of the coated lithium metal, and (b) CV curves in the first scan of the coated lithium metal at the scan rate of 0.1 mV s^{-1} (Modified from ref. 26).

1.3.2 Positive electrodes

Positive electrode materials include lithium transitional metal oxides such as $LiCoO_2$, $LiMn_2O_4$, $Li[Ni_{1/3}Co_{1/3}Mn_{1/3}]O_2$ and $LiFePO_4$, which are also used as positive electrode materials for lithium ion batteries and 1G ARLBs. They are formerly discussed in the section for the 1G ARLBs, and will not be discussed here again since their performance is similar to that discussed in Section 1.1.2. By the way, NiOOH, AgO, Ag, Cu, and $Fe(CN_6)_3^-/Fe(CN_6)_4^-$ couples, can be used as the positive electrode materials [91-95]. Recently, some redox couples based on aqueous electrolyte such as I_3^-/I^- are explored as positive electrodes [31,96]. Their electrochemical reactions are simpler and can be described as eq. (2) [96]:

$$3\,I^- \underset{\text{Discharge}}{\overset{\text{Charge}}{\rightleftharpoons}} I_3^- + 2e^- \qquad E^o = 0.536 \text{ V (vs. SHE)} \qquad (2)$$

These successful candidates have higher energy densities and reasonable charge stability. The high solubility of triiodide/iodide redox couple shows fast electrochemical reaction kinetics. Its specific capacity is 207 mAh g^{-1} at a current rate of 2.5 mA cm^{-2}. This provides a chance to build up 2G ARLBs of high energy density.

1.3.3 Electrochemical behaviors of 2G ARLBs

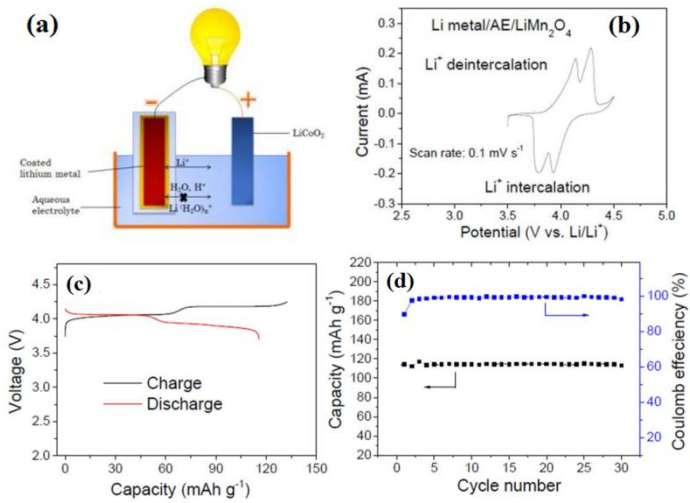

Fig.10 (a) Schematic illustration of our designed new ARLBs using the coated lithium metal as negative electrode, lithium intercalation compounds as positive electrode and aqueous solution as electrolyte, (b) CV curve of the new ARLB with $LiMn_2O_4$ as positive electrode at the scan rate of 0.1 mV s^{-1}, (c) Galvanostatic charge and discharge curves of the ARLB at the current density of 100 mA g^{-1} based on the mass of $LiMn_2O_4$ between 3.7 and 4.25 V in the first cycle, and (d) cycling behavior of the ARLB (Modified from refs. 26 and 27).

We combined the coated Li metal as mentioned above with lithium intercalation compounds such as $LiMn_2O_4$, $LiCoO_2$ and $LiFePO_4$ to build up a 2G ARLB as in Fig. 10a [26, 27, 97], whose average output voltage and energy density are markedly higher than those of the 1G ARLBs. They also present good cycling and rate performance. When $LiMn_2O_4$ is used as the positive electrode, the CV curve of the 2G ARLB presents two couples of redox peaks situated at 4.14/3.80 and 4.28/3.93 V, respectively, at the scan rate of 0.1 mV s^{-1} (Fig. 10b), which is consistent with the charge and discharge curves (Fig. 10c). It indicates that this kind of "potential cross-over", which is similar to the electrode double layer, can assemble 2G ARLBs with a stable work voltage up to 4 V, a break-through of the stable electrochemical window of water (1.23 V). Its cycling is very excellent with Coulombic efficiency of 100% except in the first cycle (Fig. 10d). Its energy density can be 446 Wh kg^{-1} based on the electrode materials, about 80% higher than that for traditional lithium ion battery. Its energy efficiency can be above 95%.

When solutions of some redox flow batteries are used as the positive electrodes, a 2G ARLB with good safety and large capacity at an acceptable cost can be easily circulated in a flow-through configuration [33, 90, 98, 99]. This new concept 2G ARLB is

different from the semi-solid redox flow batteries [100, 101] since it uses Li metal in an organic electrolyte as negative electrode and an aqueous solution of a redox-couple as the positive electrode. It has the advantages of high energy density from lithium metal and an independent operation on power and energy capacity from redox flow battery. Additionally, it also reduces self-discharge for the redox flow battery system. In the case of the 2G ARLBs based on Li//I, its energy density can be 330 Wh kg^{-1}, approximately twice that of lithium ion batteries [96]. Its power density eventually approaches 34.8 mW cm^{-2} at 12 mA cm^{-2} associated with a discharge voltage of 2.9 V. Moreover, Li//I battery exhibits excellent cycling performance, capacity retention with no degradation after 100 cycles and ideal Coulombic efficiency, superior to those of Li//air and Li//S batteries.

Briefly, the 2G ARLBs will surely be promising for energy storage systems in electric vehicles due to its low cost, much reliable safety and high energy density. It provides another chemistry for post lithium ion batteries. However there are many remaining challenges at its infancy, especially in optimizing the battery structure, searching for proper positive electrode, and improving both the ionic conductivity and stability of LISICON film at any environmental conditions such as in the full range of pH [102, 103].

2 Aqueous supercapacitors

Supercapacitors or electrochemical capacitors (ECs) are energy storage devices which can provide higher power density as compared to batteries and higher energy density than conventional capacitors. They are regarded as promising energy storage devices for electric vehicles, and have attracted intensive attentions [104-106]. Here we focus on neutral aqueous medium, *i.e.* lithium, sodium and potassium solutions in a wide range of concentrations, which are promising electrolytes for supercapacitors because they are cheap, non-corrosive and allow applying diverse current collectors, making the supercapacitor assembling process much easier and cheaper. Additionally, such electrolytes are electrochemically stable and environmentally friendly [107].

Depending on the energy storage mechanisms, supercapacitors can be classified into two general categories: electrochemical double-layer capacitors (EDLCs) and pseudocapacitors [108]. EDLCs store charges electrostatically *via* reversible ion absorption /desorption at the electrode/electrolyte interface, which commonly use carbon-based active electrode materials with high surface area [109]. In contrast, pseudocapacitors use reversible redox reactions at the surface of electroactive materials for charge storage [110]. Typical active pseudocapacitive materials include transition metal oxides and electronically conducting redox polymers such as polyaniline (PAn), polypyrrole (PPy), polythiophene (PTh) and their derivatives [57]. Here we discuss their electrode materials according to their different mechanisms.

2.1 Electrode materials based on electrochemical double layer absorption/ desorption

In neutral aqueous solutions, so far there are only carbon materials with high surface area, which display electrochemical double layered capacitive behavior. To date, various forms of carbonaceous materials such as activated carbons (ACs) [111], mesoporous carbons [112], activated carbon fabrics [113] and carbon nanotubes (CNTs) [114] have been utilized for both symmetric and asymmetric supercapacitors. These carbon-based materials offer some advantageous features including low cost, high

electronic conductivity, good electrochemical stability with long cycling life and tunable porous structures. Most recently, graphene[115] and graphene-based composites [116-118] have been investigated because of their unique structures and high specific surface area (2630 m^2 g^{-1}).

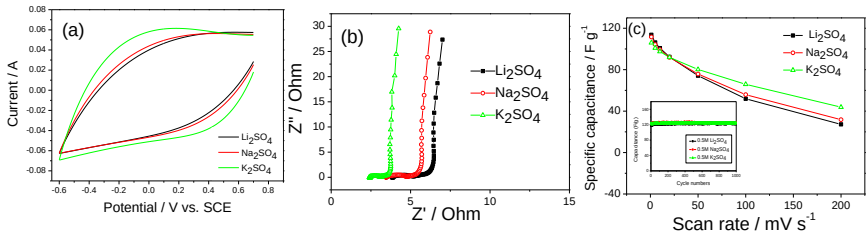

Fig. 11 (a) CV curves of AC in 0.5 mol L^{-1} aqueous Li_2SO_4, Na_2SO_4 and K_2SO_4 electrolytes at the scan rates of 100 mV s^{-1}, (b) the Nyquist plots of AC electrode at the open-circuit voltage in the three electrolytes, and (c) the change of capacitance of AC with the scan rate in the three electrolytes. The inset shows the cycling behaviors of AC in the three electrolytes (Modified from ref. 120).

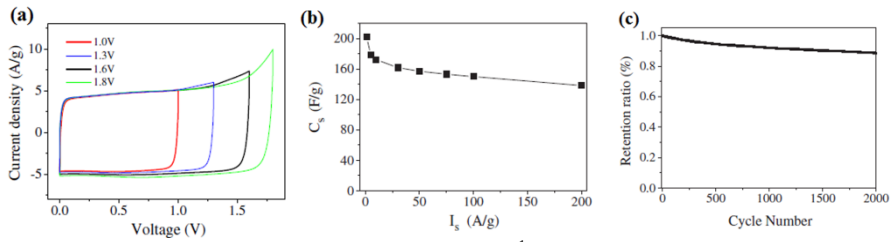

Fig. 12 (a) CV curves at the scan rates of 50 mV s^{-1} for a hydrated graphene film-based supercapacitor in 1.0 mol L^{-1} Li_2SO_4 with the maximum voltage of 1, 1.3, 1.6 and 1.8 V, (b) gravimetric capacitance of a hydrated graphene film-based supercapacitor in 1.0 mol L^{-1} Li_2SO_4 with the voltage of 1.6 V at different current densities, and (c) the cycling performance over 2000 cycles at 100 A g^{-1} with the voltage of 1.6 V (Modified from ref. 121).

In the case of ACs, the pores including micro-, meso-, and macro-pores are randomly distributed in the ACs, the pore sizes have an significant influence on capacitance which is closely related to the electrolytes[119, 120]. In neutral solutions, the ion size presents different behavior at different current or power densities. For example, in 0.5 mol L^{-1} Li_2SO_4, Na_2SO_4 and K_2SO_4 aqueous electrolytes, the rate behavior of the AC improves in the order of Li_2SO_4 < Na_2SO_4 < K_2SO_4 (Fig. 11a). This can be attributed to the different hydrated ionic radius contributing to their different charge densities and different migration speeds [120]. The hydrated ionic radius of K^+ is the smallest and its ionic conductivity is the highest, consequently its access to the inner pores of AC is much easier, and the relaxation time for the migration of the hydrated K^+ is the shortest at the high scan rate. In addition, the equivalent series resistances (ESR) for the three electrolytes decrease in the order of Li_2SO_4 > Na_2SO_4 > K_2SO_4 (Fig.11b). As a result, K_2SO_4-based electrolyte exhibits the largest capacitance at the high scan rates (Fig. 11c). At the low scan rate, the capacitance is mainly determined by the size of un-hydrated cations, which decreases in the order of Li^+ < Na^+ < K^+. As a result, the capacitance increases in the same order, i.e. Li^+ > Na^+ > K^+. They present very stable cycling at the neutral

electrolytes, which opens a platform for aqueous supercapacitors based on neutral electrolytes.

Chemical converted graphene (CCG) retains a rectangular shape at the slow scan rates in 1 mol L^{-1} Li_2SO_4 solution (Fig. 12a) [121]. The voltage is up to 1.6 and even 1.8 V when the oxygen in the Li_2SO_4 aqueous solution is removed. It also exhibits good rate and long cycling performance. A specific capacitance of 202 or 138 F g^{-1} is achieved at a galvanostatic charge/discharge rate of 1 or 200 A g^{-1}, respectively (Fig. 12b). Over 88.8% of specific capacitance is retained after 2000 cycles at a high current density of 100 A g^{-1} (Fig. 12c).

2.2 Electrode materials based on absorption/desorption and redox reactions

Any material has some specific surface area, and the absorption/desorption is not avoidable. It is well known that some transition-metal oxides such as amorphous RuO_2 [122], MnO_2 [105, 123], V_2O_5 [56, 81, 124] and MoO_3 [45, 104, 125], as well as some polymers such as PAn, PPy, PTh (polythiophene) and their derivatives exhibit pseudocapacitive properties [57]. Their large specific pseudocapacitance (typically 300-1000 F g^{-1}) exceeds that of carbon-based materials (typically 100-250 F g^{-1}) based on double layer charge storage. Of course, the positive electrode materials for ARLBs can also be good positive electrode materials for aqueous supercapacitors since they also present good and reversible redox reactions, which present good pseudocapacitance. Since they are discussed in Section 1.1.1, here it will not be repeated.

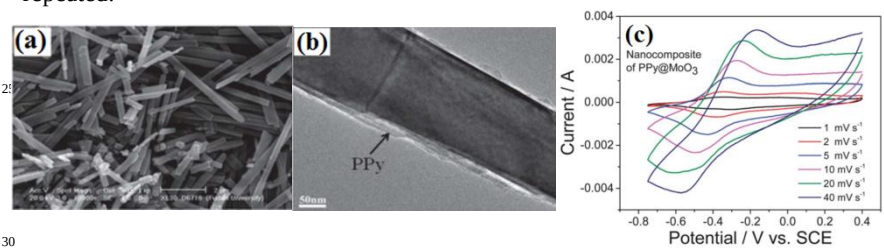

Fig. 13 (a) SEM micrographs of the virginal α-MoO_3 nanobelts and (b) TEM micrograph of the PPy@MoO_3 nanocomposite, and (c) the nanocomposite of the PPy@MoO_3 at different scan rates in 0.5 mol L^{-1} K_2SO_4 aqueous electrolyte (Modified from ref. 104).

Material morphology is closely related to the specific surface area and the diffusion of ions. Pseudocapacitive technology has benefited greatly by moving from conventional to nanostructured materials [110]. The nanostructured materials have drawn intense attention to develop better supercapacitors because of their high surface area, nanosize effects, significantly enhanced kinetics and high capacitance. For example, a nanocomposite of molybdenum trioxide [104, 126] (α-MoO_3) nanobelts coated with polypyrrole (PPy), whose morphology is shown in Figs. 13a and 13b, presents one redox peaks at -0.45 and -0.32 V (vs. SCE), respectively, correspond to the reversible intercalation/deintercalation of K^+ ions into/from the MoO_3 matrix in its CV curves (Fig. 13c), indicating a good negative electrode for supercapacitors. Even at the high scan rate of 40 mV s^{-1}, the redox peaks are still evident. Of course, the nanocomposite can also present good reversible intercalation/deintercalation of Li^+ and Na^+ ions into/from the MoO_3 matrix.

For different neutral aqueous electrolytes containing a lithium salt of $Beti^-$, $C_6H_{13}CO_2^-$, ClO_4^- or NO_3^- [127], MnO_2 presents better electrochemical performance in

the electrolytes based on a mineral lithium salt than the organic anions, including good material stability and capacity retention. MnO_2 nanorods with a surface area of 135 m^2 g^{-1} present a better capacitive behavior than its micrometer material [123]. It is similar to AC [120], MnO_2 presents the best rate capability in the K_2SO_4 aqueous electrolyte and the highest capacitance in the Li_2SO_4 one [123]. When a conductive network such as MWCNTs is introduced, their rate capability will be much improved [105]. Nanohybrids of $LiMn_2O_4$ and nanoporous $LiMn_2O_4$ can also achieve better capacitive behaviors [48,128,129].

The positive electrode materials for ARSBs and ARPBs such as Na_xMnO_2 and K_xMnO_2 can also be good positive electrode materials for supercapacitors [69-71,73]. When they exist in nanostructures such as nanowires, their capacitive behavior will be much improved.

2.3 Aqueous supercapacitors

In neutral aqueous electrolytes, symmetric supercapacitors can be assembled by using carbonaceous materials such as AC, CNTs and graphene as both electrodes [119]. In the case of supercapacitors based on graphene, its voltage range is much higher than those based on acid or basic electrolytes [121]. However, most supercapacitors are asymmetric, and some of them including their partial electrochemical performance are summarized in Table 5. Here we take the supercapacitor of AC//K_xMnO_2 nH_2O as one example.

The charge and discharge curves of the supercapacitor of AC//K_xMnO_2 nH_2O in 0.5 mol L^{-1} K_2SO_4 electrolyte at 2C rate presents slight plateaus at about 1.2 V (Fig. 14a), which is due to the K_xMnO_2 nH_2O positive electrode. It exhibits short plateaus at about 0.6 and 0.4 V (vs. SCE) during the charge and discharge process, respectively. Similar to the supercapacitor of AC//MnO_2 in neutral aqueous electrolytes [123], it also presents excellent cycling life (Fig. 14b). Without the removal of oxygen in the aqueous electrolyte, there is no clear capacitance fading after 10000 full cycles. As mentioned above, AC and MnO_2 present best rate capability in the K_2SO_4 aqueous electrolyte among the Li_2SO_4, Na_2SO_4 and K_2SO_4 aqueous electrolytes. The AC//K_xMnO_2 nH_2O supercapacitor also shows better rate capability than that based on AC//$LiMn_2O_4$. At the higher power, its energy density is higher than that based on AC//$LiMn_2O_4$ though its energy density is smaller at the lower power (Fig. 14c) [71].

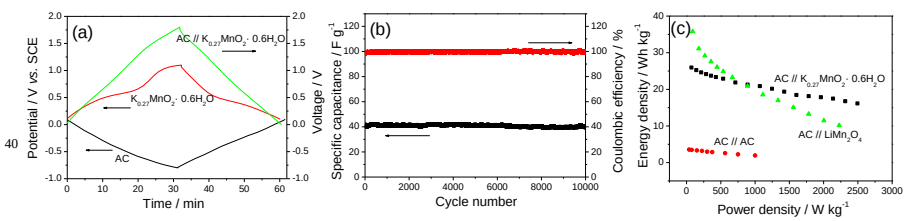

Fig. 14 (a) Charge and discharge curves of the supercapacitor of AC//$K_{0.27}MnO_2$ $0.6H_2O$ and its electrodes in 0.5 mol L^{-1} aqueous electrolytes at the scan rate of 5 mV s^{-1}, (b) cycling behavior of the supercapacitor of AC//$K_{0.27}MnO_2$ $0.6H_2O$, and (c) Ragone plot of the supercapacitor of AC//$K_{0.27}MnO_2$ $0.6H_2O$ (Modified from ref. 71).

In the case of the asymmetric supercapacitors, the weight ratios of each electrode should be optimized to assure the capacitance of the negative electrode is a

litter over than that of the positive electrode [126]. For example, in the case of the supercapacitor based on AC and PPy@MoO_3 in 0.5 mol L^{-1} K_2SO_4 electrolyte, their optimal weight ratio is 1:1.

Due to the good advantages of the neutral aqueous electrolytes, the aqueous supercapacitors based on neutral electrolytes exhibit high energy and power densities, excellent cycling life and environmental friendliness as shown in Table 5. Of course, their cost is much cheaper than those based on organic electrolytes. These exciting results offer new chances for the rapid development of supercapacitors.

3. Summary and outlooks

As the most ideal electrolyte solvent, water is abundant and environmentally friendly. The above illustration shows clearly that the latest explored energy storage systems based on neutral aqueous electrolytes provide quite a lot of advantages over the traditional energy storage systems:

- Low cost: inexpensive and good availability of salts such as Li_2SO_4 and $LiNO_3$ instead of expensive $LiPF_6$, which do not need rigorous strict humidity control of the assembling environment as batteries based on organic electrolytes and their requirements on separators are low.
- Suitable for charging and discharging at high rates: high ionic conductivity of the aqueous electrolytes.
- Satisfactory or high energy density based on both electrodes.
- High power density competitive with fuel cells and capacitors.
- Long cycling life.
- High Coulombic efficiency.
- Environmental friendliness: complete green, which is superior to lithium ion batteries having a serious pollution of HF acid to the environment due to the reaction of the used $LiPF_6$ with water.
- More safe: no combustibility or explosion comparing with the energy storage systems based on flammable organic electrolyte.

Of course, these advantages are achieved due to the new preparation technologies especially coating and nanostructures. New concepts such as aqueous rechargeable lithium batteries of high energy density (2G ARLBs) are also important to break through the electrochemical stable window of water, which provide new directions for post lithium ion batteries. Introduction of nanostructures together with the traditional intercalation compounds leads to an increase of energy and power densities and excellent cycling life of supercapacitors.

The above characteristics are also important for these systems in storing energy from electrical grids connected with intermittent energy sources such as solar, wind and hydropower. It is also important to lower the cost and meet the stringent safety requirements of batteries for pure electric vehicles. The challenges to significantly increase the specific output power and energy density of batteries are urgently needed to solve [100, 144]. Some directions are very important for the further development of energy storage systems based on neutral aqueous electrolytes:

(1) New energy storage chemistries are still needed to explore. For example, MnO_2 can be the reversible host some divalent cations such as Zn^{2+}, Mg^{2+}, Ca^{2+} and Ba^{2+} in aqueous electrolytes [130-132], and the +2 cations can suppress activation energy barrier for the interfacial charge transfer of a prussian blue analog thin film electrode [133, 134]. Al^{3+} ion also presents reversible storage behavior in anatase TiO_2 nanotube arrays [135]. The mixed system (Li,Na)$FePO_4$//$FePO_4$ is also possible [136, 137].

Aqueous rechargeable batteries such as Ni//Fe battery[138, 139], $Co(OH)_2$//$Ni(OH)_2$ [140], TiO_2//$Ni(OH)_2$ [141], and aqueous Li//S rechargeable batteries[142] have been proposed. The concept of desalination battery with a simple construction and a promising energy efficiency is fascinating since it has fewer corrosion problems than the existing desalination technology by using readily available materials [143]. Undoubtedly, such efforts are important and need more encouraging. Combination of batteries with supercapacitors is also a good way to realize the balance between energy and power densities.

(2) New materials are crucial to push forward the application of these energy storage systems. For example, solid electrolytes need much improvement in mechanical processing, ionic conductivity and stability in different aqueous electrolytes [146-149].

(3) More preparation or modification methods for electrode materials are still in need. For example, electrode materials with good crystal orientation to realize much faster charging or discharging behavior require good templates [13, 43]. Micro-/nano-structured materials with excellent electrochemical performances is another focus since nanostructures provide short diffusion pathways and large specific surface area and microstructure provides good processing and stability [144, 145].

Acknowledgment: Financial support from MOST (2010DFA61770), NSFC (21073046) and STCSM (12JC1401200) is greatly appreciated.

References:

1. B. Dunn, H. Kamath and J. M. Tarascon, *Science*, 2011, **334**, 928-935.
2. C. Liu, F. Li, L. P. Ma and H. M. Cheng, *Adv. Mater.*, 2010, **22**, E28-62.
3. X. Chen, C. Li, M. Gratzel, R. Kostecki and S. S. Mao, *Chem. Soc. Rev.*, 2012, **41**, 7909-7937.
4. J. Liu, *Adv. Funct. Mater.*, 2013, **23**, 924-928.
5. J. Liu, J. G. Zhang, Z. Yang, J. P. Lemmon, C. Imhoff, G. L. Graff, L. Li, J. Hu, C. Wang, J. Xiao, G. Xia, V. V. Viswanathan, S. Baskaran, V. Sprenkle, X. Li, Y. Shao and B. Schwenzer, *Adv. Funct. Mater.*, 2013, **23**, 929-946.
6. J. B. Goodenough and K. S. Park, *J. Am. Chem. Soc.*, 2013, **135**, 1167-1176.
7. J. Liu and X. W. Liu, *Adv. Mater.*, 2012, **24**, 4097-4111.
8. M. Wagemaker and F. M. Mulder, *Account. Chem. Res.*, 2013, **46**, 1206–1215.
9. B. Scrosati, J. Hassoun and Y. K. Sun, *Energy Environ. Sci.*, 2011, **4**, 3287-3295.
10. J. Cabana, L. Monconduit, D. Larcher and M. R. Palacin, *Adv. Mater.*, 2010, **22**, E170-E192.
11. N. S. Choi, Z. Chen, S. A. Freunberger, X. Ji, Y. K. Sun, K. Amine, G. Yushin, L. F. Nazar, J. Cho and P. G. Bruce, *Angew. Chem. Int. Ed.*, 2012, **51**, 9994-10024.
12. S. Y. Hong, Y. J. Kim, Y. W. Park, A. Choi, N. S. Choi and K. T. Lee, *Energy Environ. Sci.*, 2013, **6**, 2067-2081.
13. Q. T. Qu, L. J. Fu, X. Y. Zhan, D. Samuelis, J. Maier, L. Li, S. Tian, Z. H. Li and Y. P. Wu, *Energy Environ. Sci.*, 2011, **4**, 3985-3990.
14. W. Tang, Y. S. Zhu, Y. Y. Hou, L. L. Liu, Y. P. Wu, K. P. Loh, H. P. Zhang and K. Zhu, *Energy Environ. Sci.*, 2013, **6**, 2093-2104.
15. G. J. Wang, L. J. Fu, N. H. Zhao, L. C. Yang, Y. P. Wu and H. Q. Wu, *Angew. Chem. Int. Ed.*, 2007, **119**, 299-301.
16. C. Wessells, R. A. Huggins and Y. Cui, *J. Power Sources*, 2011, **196**, 2884-2888.
17. S. F. Tie and C. W. Tan, *Renew. Sust. Energ. Rev.*, 2013, **20**, 82-102.
18. J. M. Tarascon and M. Armand, *Nature*, 2001, **414**, 359-367.

19. M. Armand and J. M. Tarascon, *Nature*, 2008, **451**, 652-657.
20. T. H. Kim, J. S. Park, S. K. Chang, S. D. Choi, J. H. Ryu and H. K. Song, *Adv. Energ. Mater.*, 2012, **2**, 860-872.
21. J. E. Goodenough, *Account. Chem. Res.*, 2013, **46**, 1053-1061.
22. B. C. Melot and J. M. Tarascon, *Account. Chem. Res.*, 2013, **46**, 1226-1238.
23. J. Jiang, Y. Li, J. Liu, X. Huang, C. Yuan and X. W. Lou, *Adv. Mater.*, 2012, **24**, 5166-5180.
24. Y. Li, Z. Y. Fu and B. L. Su, *Adv. Funct. Mater.*, 2012, **22**, 4634-4667.
25. W. Li, J. R. Dahn and D. Wainwright, *Science*, 1994, **264**, 1115-1118.
26. X. J. Wang, Y. Y. Hou, Y. S. Zhu, Y. P. Wu and R. Holze, *Sci. Rep.*, 2013, **3**, 1401-1405.
27. X. J. Wang, Q. T. Qu, Y. Y. Hou, F. X. Wang and Y. P. Wu, *Chem. Commun.*, 2013, **49**, 6179-6181.
28. Y. G. Wang, J. Yi and Y. Y. Xia, *Adv. Energ. Mater.*, 2012, **2**, 830-840.
29. G. J. Wang, Q. T. Qu, B. Wang, Y. Shi, S. Tian, Y. P. Wu and R. Holze, *Electrochim. Acta*, 2009, **54**, 1199-1203.
30. G. J. Wang, L. C. Yang, Q. T. Qu, B. Wang, Y. P. Wu and R. Holze, *J. Solid State Electrochem.*, 2009, **14**, 865-869.
31. Y. Lu, J. B. Goodenough and Y. Kim, *J. Am. Chem. Soc.*, 2011, **133**, 5756-5759.
32. H. B. Li, M. H. Yu, F. X. Wang, P. Liu, Y. Liang, J. Xiao, C. X. Wang, Y. X. Tong and G. W. Yang, *Nat. Commun.*, 2013, **4**, 1894-1900.
33. H. P. Zhang, S. S. Liang, B. P. Sun, X. J. Yang, X. Wu and T. Yang, *J. Mater. Chem. A*, 2013, **1**, 14476-14479.
34. F. Beck and P. Ruetschi, *Electrochim. Acta*, 2000, **45**, 2467-2482.
35. H. Manjunatha, G. S. Suresh and T. V. Venkatesha, *J. Solid State Electrochem.*, 2010, **15**, 431-445.
36. J. Y. Luo, W. J. Cui, P. He and Y. Y. Xia, *Nat. Chem.*, 2010, **2**, 760-765.
37. W. Tang, L. L. Liu, S. Tian, L. Li, Y. B. Yue, Y. P. Wu and K. Zhu, *Chem. Commun.*, 2011, **47**, 10058-10060.
38. W. Tang, L. L. Liu, S. Tian, L. Li, Y. B. Yue, Y. Bai, Y. P. Wu, K. Zhu and R. Holze, *Electrochem. Commun.*, 2011, **13**, 1159-1162.
39. W. Tang, L. L. Liu, S. Tian, L. Li, Y. B. Yue, Y. P. Wu, S. Y. Guan and K. Zhu, *Electrochem. Commun.*, 2010, **12**, 1524-1526.
40. F. X. Wang, S. Y. Xiao, Z. Chang, Y. Q. Yang and Y. P. Wu, *Chem. Commun.*, 2013, **49**, 9209-9211.
41. F. X. Wang, S. Y. Xiao, Y. Shi, L. L. Liu, Y. S. Zhu, Y. P. Wu, J. Z. Wang and R. Holze, *Electrochim. Acta*, 2013, **93**, 301-306.
42. Q. T. Qu, G. J. Wang, L. L. Liu, S. Tian, Y. Shi, Y. P. Wu and R. Holze, *Funct. Mater. Lett.*, 2010, **3**, 151-154.
43. W. Tang, Y. Y. Hou, F. X. Wang, L. L. Liu, Y. P. Wu and K. Zhu, *Nano Lett.*, 2013, **13**, 2036-2040.
44. W. Tang, S. Tian, L. L. Liu, L. Li, H. P. Zhang, Y. B. Yue, Y. Bai, Y. P. Wu and K. Zhu, *Electrochem. Commun.*, 2011, **13**, 205-208.
45. W. Tang, L. L. Liu, Y. S. Zhu, H. Sun, Y. P. Wu and K. Zhu, *Energ. Environ. Sci.*, 2012, **5**, 6909-6913.
46. L. J. Fu, L. C. Yang, Y. Shi, B. Wang and Y. P. Wu, *Micropor. Mesopor. Mat.*, 2009, **117**, 515-518.
47. X. L. Wu, L. Y. Jiang, F. F. Cao, Y. G. Guo and L. J. Wan, *Adv. Mater.*, 2009, **21**, 2710-2714.

48. F. X. Wang, S. Y. Xiao, X. W. Gao, Y. S. Zhu, H. P. Zhang, Y. P. Wu and R. Holze, *J. Power Sources*, 2013, **242**, 560-565.
49. A. M. Reddy, M. M. Shaijumon, S. R. Gowda and P. M. Ajayan, *Nano Lett.*, 2009, **9**, 1002-1006.
50. X. W. Lou, D. Deng, J. Y. Lee, J. Feng and L. A. Archer, *Adv. Mater.*, 2008, **20**, 258-262.
51. C. K. Chan, H. L. Peng, G. Liu, K. Mailwarth, X. F. Zhang, R. A. Huggins and Y. Cui, *Nature*, 2008, **3**, 31-35.
52. H. L. Wang, Y. Yang, Y. Y. Liang, L. F. Cui, H. S. Casalongue, Y. G. Li, G. S. Hong, Y. Cui and H. J. Dai, *Angew. Chem.*, 2011, **123**, 7502-7503.
53. A. Q. Pan, J. G. Zhang, Z. M. Nie, G. Z. Cao, B. W. Arey, G. S. Li, S. Q. Liang and J. Liu, *J. Mater. Chem.*, 2010, **20**, 9193–9199.
54. J. S. Chen, Y. L. Tan, C. M. Li, Y. L. Cheah, D. Luan, S. Madhavi, F. Y. C. Boey, L. A. Archer and X. W. Lou, *J. Am. Chem. Soc.*, 2012, **132**, 6124–6130.
55. L. L. Liu, X. J. Wang, Y. S. Zhu, C. L. Hu, Y. P. Wu and R. Holze, *J. Power Sources*, 2013, **224**, 290-294.
56. W. Tang, X. W. Gao, Y. S. Zhu, Y. B. Yue, Y. Shi, Y. P. Wu and K. Zhu, *J. Mater. Chem.*, 2012, **22**, 20143-20145.
57. R. Holze and Y. P. Wu, *Electrochim. Acta*, 2014, doi: 10.1016/j.electacta.2013.08.100.
58. A. G. Macdiarmid, *Angew. Chem. Int. Ed.* , 2011, **40**, 2581-2590.
59. Z. G. Yin and Q. D. Zheng, *Adv.Energy Mater.*, 2012, **2**, 179-218.
60. H. Heli, H. Yadegari and A. Jabbari, *J. Phys. Chem. C*, 2011, **115**, 10889-10897.
61. G. J. Wang, Q. T. Qu, B. Wang, Y. Shi, S. Tian, Y. P. Wu and R. Holze, *J. Power Sources*, 2009, **189**, 503-506.
62. M. Minakshi, P. Singh, D. Appadoo and D. E. Martin, *Electrochim. Acta*, 2011, **56**, 4356-4360.
63. M. Minakshi, P. Singh, D. R. G. Mitchell, T. B. Issa and K. Prince, *Electrochimica Acta*, 2007, **52**, 7007-7013.
64. M. Minakshi, P. Singh, S. Thurgate and K. Prince, *Electrochem. Solid. St.*, 2006, **9**, A471-A474.
65. H. P. Zhang, X. Wu, T. Yang, S. S. Liang and X. J. Yang, *Chem. Commun.*, 2013, **49**, 9977-9979.
66. J. Yan, J. Wang, H. Liu, Z. Bakenov, D. Gosselink and P. Chen, *J. Power Sources*, 2012, **26**, 222-226.
67. V. Palomares, C. M. Casas, M. E. Castillo, M. H. Han and T. Rojo, *Energ. Environ. Sci.*, 2013, **6**, 2312-2337.
68. S. Komab, A. Ogata and T. Tsuchikawa, *Electrochem. Commun.*, 2008, **10**, 1435–1437.
69. Q. T. Qu, Y. Shi, S. Tian, Y. H. Chen, Y. P. Wu and R. Holze, *J. Power Sources*, 2009, **194**, 1222-1225.
70. J. Shao, X. Y. Li, Q. T. Qu and Y. P. Wu, *J. Power source*, 2013, **223**, 56-61.
71. Q. T. Qu, L. Li, S. Tian, W. L. Guo, Y. P. Wu and R. Holze, *J. Power Sources*, 2010, **195**, 2789-2794.
72. X. Liu, N. Zhang, J. F. Ni and L. J. Gao, *J. Solid State Electrochem.*, 2013, **17**, 1939-1944.
73. J. F. Whitacre, A. Tevar and S. Sharma, *Electrochem. Commun.*, 2010, **12**, 463-466.
74. D. J. Kim, R. Ponraj, A. G. Kannan, H.-W. Lee, R. Fathi, R. Ruffo, C. M. Mari and D. K. Kim, *J. Power Sources*, 2013, **244**, 758-763.

75. J. F. Whitacre, T. Wiley, S. Shanbhag, Y. Wenzhuo, A. Mohamed, S. E. Chun, E. Weber, D. Blackwood, B. E. Lynch, J. Gulakowski, C. Smith and D. Humphreys, *J. Power Sources*, 2012, **213**, 255-264.
76. C. D. Wessells, M. T. McDowell, S. V. Peddada, M. Pasta, R. A. Huggins and Y. Cui, *ACS Nano*, 2012, **1688-1694**.
77. M. Pasta, C. D. Wessells, R. A. Huggins and Y. Cui, *Nat. Commun.*, 2012, **3**, 1149.
78. C. D. Wessells, R. A. Huggins and Y. Cui, *Nat. Commun.*, 2011, **2**, 550.
79. C. D. Wessells, S. V. Peddada, R. A. Huggins and Y. Cui, *Nano Lett.*, 2011, **11**, 5421-5425.
80. S. H. Yu, M. Shokouhimehr, T. Hyeon and Y. E. Sung, *ECS Electrochem. Lett.*, 2013, **2**, A39-A41.
81. Q. T. Qu, Y. Shi, L. L. Li, W. L. Guo, Y. P. Wu, H. P. Zhang, S. Y. Guan and R. Holze, *Electrochem. Commun.*, 2009, **11**, 1325-1328.
82. Z. Li, D. Young, K. Xiang, W. C. Carter and Y. M. Chiang, *Adv. Energ. Mater*., 2012, 290-294.
83. S. I. Park, I. Gocheva, S. Okada and J. Yamaki, *J. Electrochem. Soc.*, 2011, **158**, A1067-A1070.
84. Z. P. Song, H. Zhan and Y. H. Zhou, *Angew. Chem. Int. Ed.* , 2010, **49**, 8622-8626.
85. W. Choi, D. Harada, K. Oyaizu and H. Nishide, *J. Am.Chem. Soc*., 2011, **133**, 19839-19843.
86. B. H. Zhang, Y. Liu, X. W. Wu, Y. Q. Yang, Z. Chang, Z. Wen and Y. P. Wu, *Chem. Commun.*, 2014, 50, 1209 - 1211.
87. Y. S. Zhu, F. X. Wang, L. L. Liu, S. Y. Xiao, Z. Chang and Y. P. Wu, *Energ. Environ. Sci.*, 2013, **6**, 618-624.
88. Y. S. Zhu, F. X. Wang, L. L. Liu, S. Y. Xiao, Y. Q. Yang and Y. P. Wu, *Sci. Rep.*, 2013, **3**, 3187.
89. H. P. Zhang, P. Zhang, Z. H. Li, M. Sun, Y. P. Wu and H. Q. Wu, *Electrochem. Commun.*, 2007, **9**, 1700-1703.
90. Y. R. Wang, P. He and H. S. Zhou, *Adv. Energ. Mater*., 2012, **2**, 770-779.
91. H. Q. Li, Y. G. Wang, H. T. Na, H. M. Liu and H. S. Zhou, *J. Am. Chem. Soc.*, 2009, **131**, 15098-15099.
92. H. Q. Li, Y. G. Wang, P. He and H. S. Zhou, *Chem. Commun.*, 2010, **46**, 2055-2057.
93. Y. G. Wang and H. S. Zhou, *Electrochem. Commun.*, 2009, **11**, 1834-1837.
94. H. S. Zhou, Y. G. Wang, H. Q. Li and P. He, *ChemSusChem*, 2010, **3**, 1009-1019.
95. T. Zhang, N. Imanishi, Y. Shimonishi, A. Hirano, Y. Takeda, O. Yamamoto and N. Sammes, *Chem. Commun.*, 2010, **46**, 1661-1663.
96. Y. Zhao, L. Wang and H. R. Byon, *Nat. Commun.*, 2013, **4**, 1896.
97. Y. Y. Hou, X. J. Wang, Y. S. Zhu, C. L. Hu, Z. Chang, Y. P. Wu and R. Holze, *J. Mater. Chem. A*, 2013, **1**, 14713-14718.
98. Y. Lu and J. B. Goodenough, *J. Mater. Chem.*, 2011, **21**, 10113-10117.
99. Y. Zhao and H. R. Byon, *Adv. Energ. Mater.*, 2013, **3**, 1529-1529.
100. Q. Huang, H. Li, M. Gratzel and Q. Wang, *Phys. Chem. Chem. Phys.*, 2013, **15**, 1793-1797.
101. M. Duduta, B. Ho, V. C. Wood, P. Limthongkul, V. E. Brunini, W. C. Carter and Y. M. Chiang, *Adv. Energ. Mater*., 2011, **1**, 511-516.
102. M. Matsuo and S. i. Orimo, *Adv. Energ. Mater.*, 2011, **1**, 161-172.
103. J. W. Fergus, *J. Power Sources*, 2010, **195**, 4554-4569.
104. Y. Liu, B. H. Zhang, Y. Q. Yang, Z. Chang, Z. B. Wen and Y. P. Wu, *J. Mater. Chem. A*, 2013, **1**, 13582-13587.

105. W. Tang, Y. Y. Hou, X. J. Wang, Y. Bai, Y. S. Zhu, H. Sun, Y. B. Yue, Y. P. Wu, K. Zhu and R. Holze, *J. Power Sources*, 2012, **197**, 330-333.
106. P. Simon and Y. Gogotsi, *Nat. Mater.*, 2008, **7**, 845-854.
107. K. Fic, G. Lota, M. Meller and E. Frackowiak, *Energ. Environ. Sci.*, 2012, **5**, 5842-5850.
108. G. H. Yu, X. Xie, L. J. Pan, Z. N. Bao and Y. Cui, *Nano Energy*, 2013, **2**, 213-234.
109. X. Li and B. Q. Wei, *Nano Energy*, 2013, **2**, 159-173.
110. Q. Lu, J. G. Chen and J. Q. Xiao, *Angew. Chem. Int. Ed.*, 2013, **52**, 1882-1889.
111. K. Fic, G. Lota, M. Meller and E. Frackowiak, *Energ. Environ. Sci.*, 2012, **5**, 5842-5850.
112. Y. Y. Lv, F. Zhang, Y. Q. Dou, Y. P. Zhai, J. X. Wang, H. J. Liu, Y. Y. Xia, B. Tu and D. Y. Zhao, *J. Mater. Chem.*, 2012, **22**, 93-99.
113. J. A. Lee, M. K. Shin, S. H. Kim, H. U. Cho, G. M. Spinks, G. G. Wallace, M. D. Lima, X. Lepro, M. E. Kozlov, R. H. Baughman and S. J. Kim, *Nat. Commun.*, 2013, **4**, 1970.
114. C. S. Du and N. Pan, *J. Power sources*, 2006, **160**, 1487-1494.
115. Y. Huang, J. J. Liang and Y. S. Chen, *Small*, 2012, **8**, 1805-1834.
116. S. Shi, C. J. Xu, C. Yang, Y. Y. Chen, J. J. Liu and F. Y. Kang, *Sci. Rep.*, 2013, **3**, 2598.
117. A. Sumboja, C. Y. Foo, X. Wang and P. S. Lee, *Adv. Mater.*, 2013, **25**, 2809-2815.
118. Q. T. Qu, S. B. Yang and X. L. Feng, *Adv. Mater.*, 2011, **23**, 5574-5580.
119. F. X. Wang, S. Y. Xiao, Y. Y. Hou, C. L. Hu, L. L. Liu and Y. P. Wu, *RSC Advances*, 2013, **3**, 13059-13084.
120. Q. T. Qu, B. Wang, L. C. Yang, Y. Shi, S. Tian and Y. P. Wu, *Electrochem. Commun.*, 2008, **10**, 1652-1655.
121. X. W. Yang, Y. S. He, G. P. Jiang, X. Z. Liao and Z. F. Ma, *Electrochem. Commun.*, 2011, **13**, 1166-1169.
122. R. R. Bi, X. L. Wu, F. F. Cao, L. Y. Jiang, Y. G. Guo and L. J. Wan, *J. Phys. Chem. C*, 2010, **114**, 2448-2451.
123. Q. T. Qu, P. Zhang, B. Wang, Y. H. Chen, S. Tian, Y. P. Wu and R. Holze, *J. Phys. Chem. C*, 2009, **113**, 14020–14027.
124. Q. T. Qu, Y. S. Zhu, X. W. Gao and Y. P. Wu, *Adv. Energ. Mater.*, 2012, **2**, 950-955.
125. T. Brezesinski, J. Wang, S. H. Tolbert and B. Dunn, *Nat. mater.*, 2010, **9**, 146.
126. Y. Liu, B. H. Zhang, S. Y. Xiao, L. L. Liu, Z. B. Wen and Y. P. Wu, *Electrochim. Acta*, 2014, **116**, 512-517.
127. A. Boisset, L. Athouël, J. Jacquemin, P. Porion, T. Brousse and M. Anouti, *J. Phys. Chem. C*, 2013, **117**, 7408-7422.
128. V. Augustyn, J. Come, M. A. Lowe, J. Kim, P. L. Taberna, S. H. Tolbert, H. D. Abruña, P. Simon and B. Dunn, *Nat. Mater.*, 2013, **12**, 518-522.
129. F. X. Wang, S. Y. Xiao, Y. S. Zhu, Z. Chang, C. L. Hu, Y. P. Wu and R. Holze, *J. Power Sources*, 2014, **246**, 19-23.
130. C. J. Xu, H. D. Du, B. H. Li, F. Y. Kang and Y. Q. Zeng, *J. Electrochem. Soc.*, 2009, **156**, A73-A78.
131. C. J. Xu, C. G. Wei, B. H. Li, F. F. Kang and Z. C. Guan, *J. Power Sources*, 2011, **196**, 7854-7859.
132. C. J. Xu, B. H. Li, H. D. Du and F. Y. Kang, *Angew. Chem. Int. Ed.*, 2012, **51**, 933-935.
133. R. Y. Wang, C. D. Wessells, R. A. Huggins and Y. Cui, *Nano Lett.*, 2013, **13**, 5748-5752.
134. Y. Mizuno, M. Okubo, E. Hosono, T. Kudo, H. Zhou and K. Ohishi, *J. Phys.Chem. C*, 2013, **117**, 10877-10882.
135. S. Liu, J. J. Hu, N. F. Yan, G. L. Pan, G. R. Li and X. P. Gao, *Energ. Environ. Sci.*, 2012, **5**, 9743-9746.

136. M. D. Levi, S. Sigalov, G. Salitra, R. Elazari, D. Aurbach, L. Daikhin and V. Presser, *J. Phys. Chem. C*, 2013, **117**, 1247-1256.
137. M. D. Levi, S. Sigalov, G. Salitra, P. Nayak, D. Aurbach, L. Daikhin, E. Perre and V. Presser, *J. Phys. Chem. C*, 2013, **117**, 15505-15514.
138. Z. Liu, S. W. Tay and X. Li, *Chem. Commun.* , 2011, **47**, 12473-12475.
139. H. L. Wang, Y. Y. Liang, M. Gong, Y. G. Li, W. Chang, T. Mefford, J. G. Zhou, J. Wang, T. Regier, F. Wei and H. J. Dai, *Nat. Commun.*, 2012, **3**, 917.
140. X. P. Gao, S. M. Yao, T. Y. Yan and Z. Zhou, *Energ. Environ. Sci.*, 2009, **2**, 502-505.
141. S. Liu, G. L. Pan, N. F. Yan and X. P. Gao, *Energ. Environ. Sci.*, 2010, **3**, 1732-1735.
142. J. Shao, X. Y. Li, L. Zhang, Q. T. Qu and H. H. Zheng, *Nanoscale*, 2013, **5**, 1460-1464.
143. M. Pasta, C. D. Wessells, Y. Cui and L. Mantia, *Nano Lett.*, 2012, **12**, 839-843.
144. Y. G. Guo, Y. S. Hu, W. Sigle and J. Maier, *Adv. Mater.*, 2007, **19**, 2087-2091.
145. L. C. Yang, Q. T. Qu, Y. Shi, Y. P. Wu and V. Ree, *ChemInform*, 2011, **42**, 39-45.
146. S. L. Chou, Y. X. Wang, J. T. Xu, J. Z. Wang, H. K. Liu and S. X. Dou, *Electrochem. Commun.*, 2013, **31**, 35-38.
147. S. Makino, Y. Shinohara, T. Ban, W. Shimizu, K. Takahashi, N. Imanishi and W. Sugimoto, *RSC Advances*, 2012, **2**, 12144-12147.
148. W. Shimizu, S. Makino, K. Takahashi, N. Imanishi and W. Sugimoto, *J. Power Sources*, 2013, **241**, 572-577.
149. T. H. Yang, X. J. Liu, L. Sang and F. Ding, *J. Power Sources*, 2013, **244**, 43-49.
150. W. Tang, X. J. Wang, Y. Y. Hou, L. L. Li, H. Sun, Y. S. Zhu, Y. Bai, Y. P. Wu, K. Zhu and T. van Ree, *J. Power Sources*, 2012, **198**, 308-311.
151. P. He, X. Zhang, Y. G. Wang, L. Cheng and Y.-Y. Xia, *J. Electrochem. Soc.*, 2008, **155**, A144-A150.
152.M. M. Rao, M. Jayalakshmi, O. Schaf, U. Guth, H. Wulff and F. Scholz, *J. Solid State Electrochem.*, 1999, **4**, 17-23.
153. H. Manjunatha, T. V. Venkatesha and G. S. Suresh, *J. Solid State Electrochem.*, 2011, **16**, 1941-1952.
154. M. S. Zhao, G. L. Huang, B. Zhang, F. Wang and X. P. Song, *J. Power Sources*, 2012, **211**, 202-207.
155. F. Wang, Y. Liu and C. Y. Liu, *Electrochim. Acta*, 2010, **55**, 2662-2666.
156. I. Stojković, N. Cvjetićanin, I. Pašti, M. Mitrić and S. Mentus, *Electrochem. Commun.*, 2009, **11**, 1512-1514.
157. H. Q. Li, T. Y. Zhai, P. He, Y. G. Wang, E. Hosono and H. S. Zhou, *J. Mater. Chem.*, 2011, **21**, 1780-1787.
158. J. Y. Luo and Y. Y. Xia, *Adv. Funct. Mater.*, 2007, **17**, 3877-3884.
159. G. J. Wang, Q. T. Qu, B. Wang, Y. Shi, S. Tian and Y. P. Wu, *ChemPhysChem*, 2008, **9**, 2299-2301.
160. C. Z. Wu, Z. P. Hu, W. Wang, M. Zhang, J. L. Yang and Y. Xie, *Chem. Commun.*, 2008, 3891-3893.
161. L. Liu, F. H. Tian, M. Zhou, H. P. Guo and X. Y. Wang, *Electrochim. Acta*, 2012, **70**, 360-364.
162. D. H. Zhou, S. Q. Liu, H. Y. Wang and G. Q. Yan, *J. Power Sources*, 2013, **227**, 111-117.
163. X. Y. Wu, Y. L. Cao, X. P. Ai, J. F. Qian and H. X. Yang, *Electrochem. Commun.*, 2013, **31**, 145-148.

Table1 Some electrode materials and their electrochemical performance for ARLBs.

Positive electrode

Materials	Potentials of redox peaks / V	Aqueous electrolytes	Theoretical capacity / mAh g^{-1}	Practical capacity / mAh g^{-1}	Retained capacity / mAh g^{-1}(rate)	Cycle retention (number/rate)	Ref.
$LiMn_2O_4$ porous	0.78/0.73, 0.92/0.85 (vs. SCE)	0.5 mol L^{-1} Li_2SO_4	148	118 (100 mA g^{-1})	90 (90C)	93%(10000/10A g^{-1})	13
nanochains				110 (500 mA g^{-1})	95 (91C)	100%(200/4.5C)	44, 150
nanotube				108 (500 mA g^{-1})	99 (91C)	100%(200/4.5C)	43
nanorods				110 (500 mA g^{-1})	97 (91C)	94%(1200/4.5C)	38
$LiCoO_2$	0.708/0.628 (vs. SCE)	0.5 mol L^{-1} Li_2SO_4	150	143 (1000 mA g^{-1})	133(70C)	100%(40/7C)	39
$LiFePO_4$	0.495/0.270 (vs. SCE)	0.5 mol $L^{-1}$$Li_2SO_4$	170	140 (1C)	96 (10C)	100%(125/4.5C)	97, 151
$Li[Ni_{1/3}Co_{1/3}Mn_{1/3}]O_2$	0.68/0.48 (vs. SCE)	2 mol L^{-1} Li_2SO_4	150	150 (1.5C)	108 (45C)	92%(50/3C)	40
$LiNiO_2$	0.76/0.2 (vs. Ag/AgCl)	0.02 mol L^{-1} LiOH	/	/			152
$LiNiPO_4$	0.094/-0.231 (vs. Hg/HgO)	saturated LiOH	170	55 (50 mA g^{-1})			62
$LiMnPO_4$	0.02/-0.3 V (vs. Hg/HgO)	saturated LiOH	170	97 (C/10)			153
$LiMn_{0.5}Fe_{0.5}PO_4$	0.34/0.32,0.92/0.86(vs. SCE)	saturated $LiNO_3$	170	123 (0.05C)			154

Negative electrode

Materials	Potentials of redox peaks / V	Aqueous electrolytes	Cycling performance	
VO_2	0.28, -0.12/-0.18 (vs. SCE)	2 mol L^{-1} LiCl	Maintaining 51% of the initial discharge capacity after 50 cycles	155
$V_2O_5 \cdot nH_2O$	0.03/0.25, 0.71/0.55 (vs. SCE)	saturated $LiNO_3$	89% of its maximal discharge capacity after 100 cycles	156
$H_2V_3O_8$	-0.43/-0.61 (vs. SCE)	5 mol L^{-1} $LiNO_3$	72% of the initial capacity after 50 cycles	157
PPy@MoO_3	-0.39/-032, -0.75/-0.59 (vs. SCE)	0.5 mol L^{-1} Li_2SO_4	90% after 150 cycles	37
PPy@LiV_3O_8	-0.28/-0.4 (vs. NHE)	0.5 mol L^{-1} Li_2SO_4	84% of the initial capacity obtained after 10 cycles	55
$LiTi(PO_4)_3$	-0.52 /-0.36 (vs. NHE)	5 mol L^{-1} $LiNO_3$	82% after 200 cycles	158
PPy	-0.2/-0.38 (vs. SCE)	0.5 mol L^{-1} Li_2SO_4		159

Table2 Rate capability and cycling performance of some nano positive electrode materials for ARLBs.

Materials	Rate and cycling performance			Ref.
	Retained capacity	Rate	Cycling	
Porous $LiMn_2O_4$	90 mAh g^{-1}	90C	93% retained after 10 000 cycles at 10 Ag^{-1}	13
$LiMn_2O_4$ nanochains	95 mAh g^{-1}	91C	No evident capacity fading after 200 cycles at 4.5 C	44
$LiMn_2O_4$ nanotube	99 mAh g^{-1}	10A g^{-1}	No definite capacity loss after 1200 cycles at 4.5 C	44
$LiMn_2O_4$ nanorods	97 mAh g^{-1}	90C	94% capacity retention after 1200 cycles at 4.5 C	38
$LiCoO_2$ nanoparticles	132 mAh g^{-1}	70C	reversible capacity increase for 40 cycles	39
Nanoporous $Li[Ni_{1/3}Co_{1/3}Mn_{1/3}]O_2$	108 mAh g^{-1}	45C	92% of the initial capacity is maintained after 50 cycles when charged at 80 C and discharged at 3 C	40
$LiFePO_4$ nanoparticles	96 mAh g^{-1}	10C	No evident capacity fading after 125 cycles at 4.5 C	97

5

Table 3 Properties of some ARLBs at different test conditions.

Battery systems	Aqueous solution	Reversible discharge capacity / mAh g^{-1}	Current density or rate	Capacity performance	Ref.
LiV_3O_8//$LiCoO_2$	Saturated $LiNO_3$	36	3.4 mA cm^{-2}	65% retention after 40 cycles	15
VO_2//$LiMn_2O_4$	5 mol L^{-1} $LiNO_3$ and 0.001 mol L^{-1} LiOH	62	60 mA g^{-1}	74% after 50 cycles	160
$LiTi_2(PO_4)_3$//$LiFePO_4$	1 mol L^{-1} Li_2SO_4	55	6C	90% after 1000 cycles	36
$LiTi_2(PO_4)_3$//$LiMnPO_4$	5 mol L^{-1} $LiNO_3$	84	0.2 mA cm^{-2}	80% after 50 cycles	153
PPy//$LiMn_2O_4$	saturated Li_2SO_4	45	0.2 mA cm^{-2}	no evident fading during the first 22 cycles	159
PPy//$LiCoO_2$	saturated Li_2SO_4	52.2	0.1C	no evident capacity fading during 120 cycles,	30
dopingPAn//$LiMn_2O_4$	Saturated $LiNO_3$	89.9 (at the 150th cycle)	75 mA g^{-1}	Increasing during initial 52 cycles, then slightly decreases	161
V_2O_5@MWCNTcoatedPPy//$LiMn_2O_4$	0.5 mol L^{-1} Li_2SO_4	110	200 mA g^{-1}	no evident capacity loss after 500 cycles	56
PPy@MoO_3//$LiMn_2O_4$	0.5 mol L^{-1} Li_2SO_4	95	500 mA g^{-1}	no more than 10% capacity loss after 150 cycles	45
Sn//$LiNiPO_4$	LiOH	55	0.5 mA cm^{-2}	a stable value of 50mAh/g after 25 cycles	62
Zn//MnO_2	saturated LiOH containing 1 mol L^{-1} $ZnSO_4$	135	0.5 mA cm^{-2}	52% after 45 cycles	63
Zn//$LiMn_2O_4$	3 mol L^{-1} LiAc and 4 mol L^{-1} $ZnAc_2$		4C	90% after 1000 cycles	66
Zn//$LiFePO_4$	15 wt% LiAc + 15 wt% $ZnAc_2$	112	1C	no evident capacity fading during 125 cycles,	65
$Na_2V_6O_{16}$//$LiMn_2O_4$	saturated Li_2SO_4	82	300 mA g^{-1}	77% after 200 cycles	162

Table 4 Cycling properties of some ARSBs under different test conditions.

Systems	Voltage / V	Energy density based on two electrode materials / $Wh \cdot kg^{-1}$	Capacity retention (cycle number)	Ref.
$NaTi_2(PO_4)_3//Na_{0.44}MnO_2$	1.10	33	60% (700)	82
$NaTi_2(PO_4)_3//Na_2NiFe(CN)_6$	1.27	43	88% (250)	163
$Zn//Na_{0.95}MnO_2$	1.50	78	92% (1000)	86
$PPy@MoO_3//Na_{0.35}MnO_2$	1.10	20	78% (1000)	126

5

Table 5 Energy and power densities and cycling performance of some aqueous supercapacitors.

System	Electrolyte	Energy density (power density)	Rate behavior	Capacity retention (cycle number)	Ref.
AC//MnO_2@NWCNT	0.5 mol L^{-1} Li_2SO_4	17.8 Wh kg^{-1} (3.34 kW kg^{-1})	0.5 A g^{-1}	100% (13000)	105
AC//V_2O_5	0.5 mol L^{-1} K_2SO_4	29Wh kg^{-1} (70 W kg^{-1})	10C	100(83%)	81
AC//Nanoporous $LiMn_2O_4$	0.5 mol L^{-1} Li_2SO_4	44.5 Wh kg^{-1} (240 W kg^{-1})	12A g^{-1}	1500(100%)	48
AC//$LiMn_2O_4$ nanohybrid	0.5 mol L^{-1} Li_2SO_4	29.8 Wh kg^{-1} (90 W kg^{-1})	3 A g^{-1}	1000(91%)	129
AC//$Na_{0.44}MnO_2$	1 mol L^{-1} Na_2SO_4		3C	1000(100%)	73
AC//$NaMnO_2$	0.5 mol L^{-1} Na_2SO_4	19.5 Wh kg^{-1} (135W kg^{-1})	10C	10000(97%)	69
AC//$K_{0.27}MnO_2$ $0.6H_2O$	0.5 mol L^{-1} K_2SO_4	17.6 Wh kg^{-1} (2 kW kg^{-1})	25C	10000(99%)	71
PPy@V_2O_5//AC	0.5 mol L^{-1} K_2SO_4	24 Wh kg^{-1} (2.5 kW kg^{-1})	10C	10000(82.5%)	124
PPy@MoO_3//AC	0.5 mol L^{-1} K_2SO_4	24 Wh kg^{-1} (150 W kg^{-1})	0.5 A g^{-1}	600(87%)	104

5

Table of Content

Green energy storage chemistries based on neutral aqueous electrolytes

Zheng Chang, Yaqiong Yang, Minxia Li, Xiaowei Wang and Yuping Wu*

Recent progress of energy storage systems based on neutral aqueous electrolytes provides quite some green chemistries as promising applications in electric vehicles and smart grids.